JACS
JOURNAL OF THE AMERICAN CHEMICAL SOCIETY

Article

Introduction of Functionality, Selection of Topology, and Enhancement of Gas Adsorption in Multivariate Metal–Organic Framework-177

Yue-Biao Zhang, Hiroyasu Furukawa, Nakeun Ko, Weixuan Nie, Hye Jeong Park, Satoshi Okajima, Kyle E. Cordova, Hexiang Deng, Jaheon Kim, and Omar M. Yaghi

J. Am. Chem. Soc., **Just Accepted Manuscript** • DOI: 10.1021/ja512311a • Publication Date (Web): 03 Feb 2015

Introduction of Functionality, Selection of Topology, and Enhancement of Gas Adsorption in Multivariate Metal–Organic Framework-177

Yue-Biao Zhang,[†] Hiroyasu Furukawa,[†] Nakeun Ko,[‡] Weixuan Nie,[†] Hye Jeong Park,[‡] Satoshi Okajima,[†] Kyle E. Cordova,[†,□] Hexiang Deng,*[,†,§] Jaheon Kim,*[,‡] and Omar M. Yaghi*[,†,¶]

[†]Department of Chemistry, University of California–Berkeley, Materials Sciences Division, Lawrence Berkeley National Laboratory, and Kavli Energy NanoSciences Institute at Berkeley, University of California–Berkeley, Berkeley, California 94720, United States

[‡]Department of Chemistry, Soongsil University, Seoul 156-743, Republic of Korea

[§]College of Chemistry and Molecular Sciences, Wuhan University, Wuhan 430072, P. R. China

[□]Center for Molecular and NanoArchitecture, Vietnam National University, Ho Chi Minh City 721337, Vietnam

[¶]King Abdulaziz City for Science and Technology, Riyadh 11442, Saudi Arabia

ABSTRACT: Metal–organic framework-177 (MOF-177) is one of the most porous materials whose structure is composed of octahedral $Zn_4O(\text{-}COO)_6$ and triangular 1,3,5-benzenetribenzoate (BTB) units to make a three-dimensional extended network based on the **qom** topology. This topology violates a long-standing thesis where highly symmetric building units are expected to yield highly symmetric networks. In the case of octahedron and triangle combination, MOFs based on the pyrite (**pyr**) and rutile (**rtl**) nets were expected instead of **qom**. In this study, we have made twenty-four MOF-177 structures with different functional groups on the triangular BTB linker having one or more functionalities. We find that the position of the functional groups on the BTB unit allows the selection for a specific net (**qom**, **pyr** and **rtl**), and that mixing of functionalities (-H, -NH_2, and $\text{-C}_4\text{H}_4$) is an important strategy for the incorporation of a specific functionality (-NO_2) into MOF-177 where otherwise incorporation of such functionality would be difficult. Such mixing of functionalities to make multivariate MOF-177 structures leads to enhancement of hydrogen uptake by 25%.

INTRODUCTION

Generally, in the reticular chemistry of metal–organic frameworks (MOFs)[1] where highly symmetric building units are used, MOFs having the most symmetric nets are expected to form (termed default nets). An analysis of MOFs in the Cambridge Structural Database revealed that over 80% of all structures belong to a handful of these default nets.[2] For example, the assembly of tetrahedra usually leads to MOFs having the diamond net,[3] and the assembly of triangles gives the silicon net of $SrSi_2$;[4] both of these nets are the default nets for the assembly of tetrahedra or triangles and they happen to be the most symmetric nets among a large number of possible nets. Indeed, this principle of high symmetry and default nets is applicable to the assembly of MOFs from other shapes as well as those involving mixed shapes, and it has become a useful guide in the design and synthesis of MOFs.[5] One of the most striking exceptions to this principle is the structure of MOF-177, which is constructed from the octahedral $Zn_4O(\text{-}COO)_6$ and triangular 1,3,5-benzenetribenzoate (BTB) units to form the **qom** net, a lower symmetry net,[6] instead of one of the default high symmetry nets (Scheme 1), pyrite (**pyr**) or rutile (**rtl**). The importance of this observation is underlined by the pervasiveness of the **qom** net when linking these shapes and expanding them as is the case with its isoreticular forms, MOF-180 and MOF-200.[7] Furthermore, MOFs based on **qom** are found to have ultrahigh porosity and exhibit useful gas storage behavior.[8] This is in contrast to the unexceptional behavior exhibited by MOFs based on the default nets (**pyr** and **rtl**).[9] Therefore, we sought to investigate this system with the aim of (a) elaborating our original thesis of high-symmetry and default nets, (b) providing insight into the design principles of MOFs, and (c) showing how these could be used to further improve properties of MOF-177 and other related systems.

In this study, we present two approaches in which we assess the tolerance of the **qom** net to functionalization of the organic linker and the mixing of linkers bearing different functionalities. We find that the position of functional groups on the linker is critical in selecting for **qom** net versus **pyr** and **rtl** nets, and that mixing of linkers exclusively affords the **qom** net. Specifically, eleven derivatives of the BTB linker (BTB-X: -H, **A**; -NH_2, **B**; -NO_2, **C**; -OCH_3, **D**; $\text{-OC}_7\text{H}_7$, **E**; -(F)_2, **F**; $\text{-C}_4\text{H}_4$, **G**; -F, **H**; -CH_3, **I**; -*m*NH_2, **J**; $\text{-C}_4\text{H}_4/\text{NH}_2$, **K** in Scheme 2, respectively) were designed and synthesized. With the exception of linker **C**, all linkers have been successfully used alone to make isoreticular MOF-177 structures. Single-crystal X-ray structures of the obtained MOF-177-X (X = **B**, **D**, **E**, **F**, **G**, **H**, **I**, **J**, and **K**; Scheme 2) were found to have 3D frameworks with the same underlying **qom** net, yet bared different functionalities. When using linker **F** or **J** alone, isomeric MOFs based on the **pyr** (MOF-155-F and MOF-155-J) or **rtl** (MOF-156-J) nets

with the same framework formula of $Zn_4O(BTB\text{-}X)_2$ were also observed as a second phase or byproduct. Furthermore, by mixing two or three different type of linkers, fourteen multivariate (MTV)[10] MTV-MOF-177 derivatives with the same underlying **qom** net, but with varied ratios of incorporated functionalities were prepared (Scheme 2): MTV-MOF-177-AB, $Zn_4O(BTB)_{1.43}(BTB\text{-}NH_2)_{0.57}$; -AC, $Zn_4O(BTB)_{1.69}(BTB\text{-}NO_2)_{0.31}$; -AD, $Zn_4O(BTB)_{1.37}(BTB\text{-}OCH_3)_{0.63}$; -AE, $Zn_4O(BTB)_{1.54}(BTB\text{-}OC_7H_7)_{0.46}$; -AF1, $Zn_4O(BTB)_{1.46}[BTB\text{-}(F)_2]_{0.54}$; -AF2, $Zn_4O(BTB)_{1.21}[BTB\text{-}(F)_2]_{0.79}$; -AG, $Zn_4O(BTB)_{1.29}(BTB\text{-}C_4H_4)_{0.71}$; -AH, $Zn_4O(BTB)_{1.17}(BTB\text{-}F)_{0.83}$; -AI, $Zn_4O(BTB)_{1.17}(BTB\text{-}CH_3)_{0.83}$; -AJ, $Zn_4O(BTB)_{1.40}(BTB\text{-}m NH_2)_{0.60}$; -BC, $Zn_4O(BTB\text{-}NH_2)_{1.18}(BTB\text{-}NO_2)_{0.82}$; -BG, $Zn_4O(BTB\text{-}NH_2)_{1.04}(BTB\text{-}C_4H_4)_{0.96}$; -CG, $Zn_4O(BTB\text{-}NO_2)_{0.62}(BTB\text{-}C_4H_4)_{1.38}$; and -ABG, $Zn_4O(BTB)_{1.03}(BTB\text{-}NH_2)_{0.31}(BTB\text{-}C_4H_4)_{0.66}$. The crystal structures and chemical formulae of these MTV-MOF-177 derivatives were determined by elemental analysis, powder X-ray diffraction (PXRD) techniques, and ^{1}H nuclear magnetic resonance (NMR) spectroscopy. Among them, five fully functionalized MOF-177 (MOF-177-B, -D, -F, and -I) analogs and seven MTV-MOF-177 (MTV-MOF-177-AB, -AD, -AE, -AF1, -AF2, -AH, and -ABG) derivatives were selected for gas adsorption studies and their performance was compared with the parent, unfunctionalized MOF-177 architecture (MOF-177-A). MOF-177-B and MOF-177-D exhibit 25% higher volumetric hydrogen uptake than that of MOF-177-A.

Scheme 1.[a]

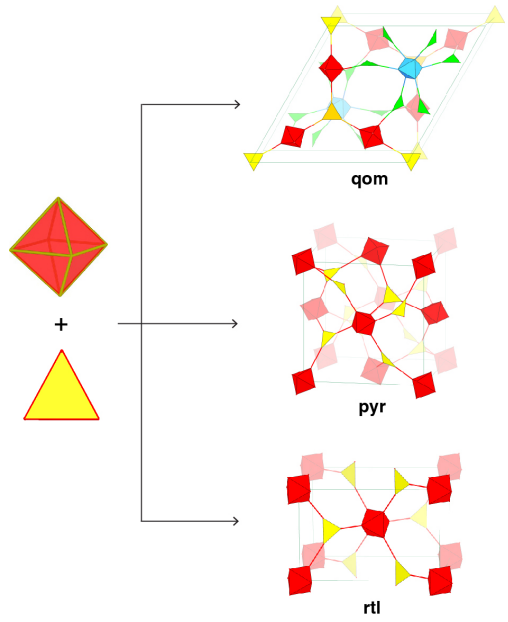

[a]Three possible (6,3)-coordinated nets formed from octahedra and triangles building units with alternative arrangement. **pyr** and **rtl** are two of the default (6,3)-coordinated nets that have only two kind of vertices and one kind of edge, and two kind of vertices and two kind of edges, respectively. **qom** is the underlying net in MOF-177 that has five kind of vertices (three triangles and two octahedra) and five kind of edges.

EXPERIMENTAL SECTION

Starting Materials and General Procedures. Zinc nitrate hexahydrate, $Zn(NO_3)_2{\cdot}6H_2O$, was purchased from Fisher Scientific; anhydrous *N,N*-dimethylformamide (DMF) was obtained from EMD Chemicals; anhydrous acetone (purity ≥ 99.8%, extra dry with AcroSeal) was purchased from Acros Organics; chloroform (pentene stabilized, HPLC grade) and anhydrous dichloromethane (purity ≥ 99.8%; amylene stabilized) were purchased from Sigma-Aldrich Co. and Fisher Scientific, respectively. *N,N*-Diethylformamide (DEF) was provided by BASF SE (Ludwigshafen, Germany), which was further purified through treatment with charcoal followed by reduced-pressure distillation. H_3BTB was purchased from TCI America. The H_3BTB functionalized linkers were prepared through Suzuki-Miyaura coupling reactions as detailed in the Supporting Information (SI, Section S1). All starting materials and solvents, except DEF, were used without further purification.

^{1}H NMR spectra were acquired on a Bruker AVB-400 NMR spectrometer. Elemental microanalyses (EA) were performed in the Microanalytical Laboratory of the College of Chemistry at UC Berkeley, using a Perkin Elmer 2400 Series II CHNS elemental analyzer. Mass spectra (MS) were obtained from the chemistry mass spectrometry facility in the QB3 Laboratory at UC Berkeley. Attenuated total reflectance Fourier transform infrared (ATR-FTIR) spectra of neat samples were recorded on a Bruker ALPHA Platinum ATR-FTIR Spectrometer equipped with a single reflection diamond ATR module. Thermal gravimetric analysis (TGA) curves were taken using a TA Q500 thermal analysis system with the heating rate of 5 °C/min under N_2 or air flow (SI, Section S4). Low-pressure adsorption isotherms were recorded on a Quadrasorb-SI or an Autosorb-1 (Quantachrome) volumetric gas adsorption analyzer. Liquid nitrogen and argon baths were used for the measurements at 77 and 87 K, respectively. Ultra-high-purity grade N_2, Ar, and H_2 gases (Praxair, 99.999% purity) were used for the adsorption measurements. Helium (Praxair, 99.999% purity) was used for the estimation of dead space throughout all adsorption measurements.

X-ray Diffraction Analyses. Single-crystal X-ray diffraction (SXRD) data of MOFs, unless otherwise mentioned, were collected on a Bruker diffractometer using Cu Kα radiation (λ = 1.54178 Å). Diffraction data for MOF-177-G was collected in the beamline 11.3.1 of the Advanced Light Source at Lawrence Berkeley National Laboratory, and diffraction data for MOF-156, MOF-157, and MOF-177-J were collected in Pohang Accelerator Laboratory (Republic of Korea) using synchrotron radiation. Powder X-ray diffraction (PXRD) patterns were recorded using a Bruker D8 Advance diffractometer with Cu Kα radiation (λ = 1.54056 Å).

General Preparation and Activation of MOF Materials. To minimize the number of factors (including concentration, solvent, temperature, and time of reaction) that can affect the formation of the **qom** topology, syntheses of the isoreticular MOF-177-X and MTV-MOF-177 compounds were carried out under similar reaction conditions as those employed for MOF-177-A (i.e. parent MOF-177). In general, these MOFs were prepared by solvothermal reaction of a mixture containing the appropriate BTB linker(s), $Zn(NO_3)_2{\cdot}6H_2O$, and DEF. However, to improve the quality of crystals, concentration of starting materials, solvent, reaction temperature, and/or reaction time were slightly modified as required. The resulting crystalline products were isolated by decanting the mother liquor and were subsequently washed with fresh solvent.

Scheme 2.[a]

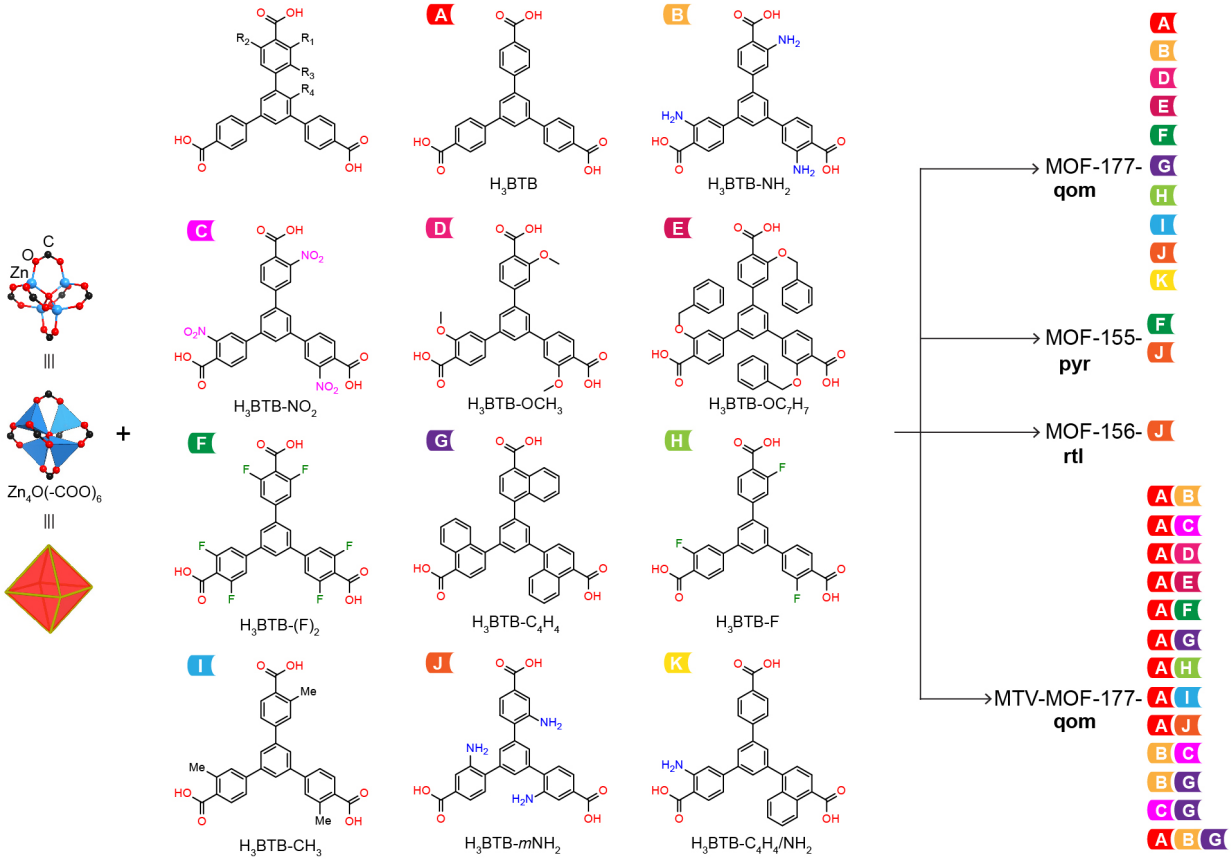

[a]BTB linkers with various functional groups at selected positions and the corresponding MOFs formed either by pure linker or mixing of various linkers. H_3BTB (**A**); $H_3BTB\text{-}NH_2$, 1,3,5-tris(3-amino-4-carboxyphenyl)benzene (**B**); $H_3BTB\text{-}NO_2$, 1,3,5-tris(3-nitro-4-carboxyphenyl)benzene (**C**); $H_3BTB\text{-}OCH_3$, 1,3,5-tris(3-methoxy-4-carboxyphenyl)benzene (**D**); $H_3BTB\text{-}OC_7H_7$, 1,3,5-tris(3-benzyloxy-4-carboxyphenyl)benzene (**E**); $H_3BTB\text{-}(F)_2$, 1,3,5-tris(3,5-difluoro-4-carboxyphenyl)benzene (**F**); $H_3BTB\text{-}C_4H_4$, 1,3,5-tris(4-carboxy-naphthalen-1-yl)benzene (**G**); H_3BTB-F, 1,3,5-tris(3-fluoro-4-carboxyphenyl)benzene (**H**); $H_3BTB\text{-}CH_3$, 1,3,5-tris(3-methyl-4-carboxyphenyl)benzene (**I**); $H_3BTB\text{-}m NH_2$, 1,3,5-tris(2-amino-4-carboxyphenyl)benzene, (**J**); $H_3BTB\text{-}C_4H_4/NH_2$, 1-(3-amino-4-carboxyphenyl)-3-(4-carboxyphenyl)-5-(4-carboxynaphthalen-1-yl)-benzene (**K**).

Removal of guest molecules within the MOF materials' pores began with a solvent exchange procedure that included immersing the as-synthesized samples into anhydrous DMF (typically 10 mL) and refreshing the DMF three times over the course of three days. Further solvent exchange, but this time with low boiling point solvents, was carried out in a similar fashion (three times over the course of three days). For typical activation,[11] a MOF sample was fully exchanged with chloroform or dichloromethane (10 mL) and evacuated at room temperature for 6 h and at 100 °C for an additional 18 h. For supercritical CO_2 drying (SCD) activation,[12] a MOF sample was fully immersed in anhydrous acetone and thoroughly exchanged with liquid CO_2 in the chamber of a Tousimis Samdri PVT-3D critical point dryer. The sample was subsequently kept in a supercritical CO_2 atmosphere (typical conditions of 35 °C and 1200 psi) for 30 min and then the supercritical CO_2 was slowly vented at room temperature over the course of several hours.

MOF-177-A, $Zn_4O(BTB)_2$. The synthesis of the parent MOF-177 structure constructed from unfunctionalized H_3BTB and $Zn(NO_3)_2{\cdot}6H_2O$ was carried out according to a published procedure.[6]

MOF-177-B, $Zn_4O(BTB\text{-}NH_2)_2$. A mixture of the acid form of **B** (12 mg, 0.025 mmol) and $Zn(NO_3)_2{\cdot}6H_2O$ (63 mg, 0.22 mmol) was dissolved in 10 mL of DEF in a 20 mL vial, which was heated at 85 °C for 48 h. Yellow block-shaped crystals were isolated and washed with DEF (3 × 5 mL). To yield guest-free material, the as-synthesized washed sample was fully exchanged with anhydrous DMF (3 × 10 mL for 3 days), followed with anhydrous acetone (3 × 10 mL for 3 days), and finally activated by the SCD method. EA for the activated sample of MOF-177-B: Calcd. for $Zn_4C_{54}H_{42}N_6O_{13} = Zn_4O(BTB\text{-}NH_2)_2$: C, 52.37; H, 2.93; N, 6.79%. Found: C, 50.12; H, 3.36; N, 5.57%.

MOF-177-C. The synthesis of MOF-177-C was unsuccessful even after extensive efforts were undertaken involving the manipulation of all the synthetic variables mentioned above.

MOF-177-D, $Zn_4O(BTB\text{-}OCH_3)_2$. A mixture of the acid form of **D** (53 mg, 0.10 mmol) and $Zn(NO_3)_2{\cdot}6H_2O$ (250 mg, 0.840 mmol) was dissolved in 10 mL DEF in a 20 mL vial, which was heated at 100 °C for 20 h. Colorless block-shaped crystals were

isolated and washed with DEF (3 × 5 mL). To yield guest-free material, the as-synthesized sample was fully exchanged with chloroform (3 × 10 mL for 3 days) and further activated by the conventional method. EA for the activated sample of MOF-177-D: Calcd. for $Zn_4C_{60}H_{42}O_{19}$ = $Zn_4O(BTB\text{-}OCH_3)_2$: C, 54.24; H, 3.19%; Found: C, 52.67; H, 2.59; N, < 0.2%.

MOF-177-E, $Zn_4O(BTB\text{-}OC_7H_7)_2$. A mixture of the acid form of **E** (76 mg, 0.10 mmol) and $Zn(NO_3)_2{\cdot}6H_2O$ (250 mg, 0.840 mmol) was dissolved in 10 mL DEF in a 20 mL vial, which was heated at 100 °C for 20 h. Colorless block-shaped crystals were isolated and washed with DEF (3 × 5 mL). EA for the as-synthesized sample of MOF-177-E: Calcd. for $Zn_4C_{161}H_{209}N_{13}O_{32}$ = $Zn_4O(BTB\text{-}OC_7H_7)_2{\cdot}(DEF)_{13}$: C, 62.38; H, 6.80; N, 5.87%. Found: C, 61.52; H, 6.93; N, 5.98%.

MOF-177-F, $Zn_4O[BTB\text{-}(F)_2]_2$. A mixture of the acid form of **F** (27 mg, 0.050 mmol) and $Zn(NO_3)_2{\cdot}6H_2O$ (125 mg, 0.420 mmol) was dissolved in 10 mL DEF in a 20 mL vial, which was heated at 100 °C for 48 h. Colorless block-shaped crystals were isolated and washed with DEF (3 × 5 mL). To yield guest-free material, the as-synthesized sample was fully exchanged with anhydrous dichloromethane (3 × 10 mL for 3 days) and further activated by the conventional method. EA for the activated MOF-177-F: Calcd. for $Zn_4C_{54}H_{18}O_{13}F_{12}$ = $Zn_4O[BTB\text{-}(F)_2]_2$: C, 47.54; H, 1.33%. Found: C, 47.03; H, 0.91; N, < 0.2%.

MOF-177-G, $Zn_4O(BTB\text{-}C_4H_4)_2$. A mixture of the acid form of **G** (30 mg, 0.050 mmol) and $Zn(NO_3)_2{\cdot}6H_2O$ (125 mg, 0.420 mmol) was dissolved in 10 mL DEF in a 20 mL vial, which was heated at 100 °C for 48 h. Colorless block-shaped crystals were isolated and washed with DEF (3 × 5 mL for 3 days). EA for the as-synthesized sample of MOF-177-G: Calcd. for $Zn_4C_{158}H_{218}N_{16}O_{29}$ = $Zn_4O(BTB\text{-}C_4H_4)_2{\cdot}(DEF)_{16}$: C, 61.87; H, 7.16; N, 7.31%. Found: C, 60.36; H, 7.42; N, 7.59%.

MOF-177-H, $Zn_4O(BTB\text{-}F)_2$. A mixture of the acid form of **H** (30 mg, 0.050 mmol) and $Zn(NO_3)_2{\cdot}6H_2O$ (125 mg, 0.420 mmol) was dissolved in 10 mL DEF in a 20 mL vial, which was heated at 100 °C for 48 h. Colorless block-shaped crystals were isolated and washed with DEF (3 × 5 mL for 3 days). EA for the as-synthesized sample of MOF-177-H: Calcd. for $Zn_4C_{129}H_{189}N_{15}O_{28}F_6$ = $Zn_4O(BTB\text{-}F)_2{\cdot}(DEF)_{15}$: C, 55.86; H, 6.87; N, 7.58%. Found: C, 54.71; H, 6.60; N, 7.63%.

MOF-177-I, $Zn_4O(BTB\text{-}CH_3)_2$. A mixture of the acid form of **I** (24 mg, 0.050 mmol) and $Zn(NO_3)_2{\cdot}6H_2O$ (125 mg, 0.420 mmol) was dissolved in 10 mL DEF in a 20 mL vial, which was heated at 100 °C for 48 h. Colorless block-shaped crystals were isolated and washed with DEF (3 × 5 mL). To yield guest-free material, the as-synthesized sample was fully exchanged with anhydrous dichloromethane (3 × 10 mL for 3 days) and further activated by the conventional method. EA for the activated MOF-177-I: Calcd. for $Zn_4C_{60}H_{42}O_{13}$ = $Zn_4O(BTB\text{-}CH_3)_2$: C, 58.47; H, 3.43%. Found: C, 56.12; H, 2.73; N, < 0.2%.

MOF-177-J, $Zn_4O(BTB\text{-}m NH_2)_2$. A mixture of the acid form of **J** (44 mg, 0.090 mmol) and $Zn(NO_3)_2{\cdot}6H_2O$ (200 mg, 0.672 mmol) was dissolved in a mixture of DMF/NMP/EtOH (7.5 mL/7.5 mL/1.5 mL) in a 20 mL vial, which was heated at 95 °C for 24 h. Yellow hexagonal plate crystals were isolated and washed with DMF (3 × 5 mL). EA for the activated sample of MOF-177-J: Calcd. for $Zn_4C_{54}H_{42}N_6O_{13}$ = $Zn_4O(BTB\text{-}m NH_2)_2$: C, 52.37; H, 2.93; N, 6.79%. Found: C, 51.63; H, 3.05; N, 6.75%.

MOF-177-K, $Zn_4O(BTB\text{-}C_4H_4/NH_2)_2$. A mixture of the acid form of **K** (25 mg, 0.050 mmol) and $Zn(NO_3)_2{\cdot}6H_2O$ (125 mg, 0.420 mmol) was dissolved in 10 mL DEF in a 20 mL vial, which was heated at 100 °C for 48 h. Yellow block-shaped crystals were isolated and washed with DEF (3 × 5 mL).

MOF-155-F, $Zn_4O[BTB\text{-}(F)_2]_2$. A mixture of the acid form of **F** (54 mg, 0.10 mmol) and $Zn(NO_3)_2{\cdot}6H_2O$ (250 mg, 0.840 mmol) was dissolved in 10 mL DEF in a 20 mL vial, which was heated at 85 °C for 48 h. Colorless cubic-shaped crystals were isolated and washed with DEF (3 × 5 mL).

MOF-155-J, $Zn_4O(BTB\text{-}m NH_2)_2$. A mixture of the acid form of **J** (54 mg, 0.10 mmol) and $Zn(NO_3)_2{\cdot}6H_2O$ (250 mg, 0.840 mmol) was dissolved in 10 mL DMF in a 20 mL vial, which was heated at 85 °C for 48 h. Colorless cubic-shaped crystals were isolated as a byproduct of MOF-177-J.

MOF-156-J, $Zn_4O(BTB\text{-}m NH_2)_2$. A mixture of the acid form of **J** (43.5 mg, 0.090 mmol) and $Zn(NO_3)_2{\cdot}6H_2O$ (200 mg, 0.672 mmol) was dissolved in DEF/MeOH (15 mL/1.5 mL) in a 20-mL vial, which was heated at 95 °C for 24 h. Yellow rod-shaped crystals were isolated and washed with DMF (3 × 20 mL). EA for the activated sample of MOF-156-J: Calcd. for $Zn_4C_{54}H_{42}N_6O_{13}$ = $Zn_4O(BTB\text{-}m NH_2)_2$: C, 52.37; H, 2.93; N, 6.79%. Found: C, 51.66; H, 2.96; N, 6.57%.

MTV-MOF-177-XY (XY = AB, AC, AD, AE, AF1, AG, AH, AI, AJ, BC, BG, and CG), $Zn_4O(BTB\text{-}X)_n(BTB\text{-}Y)_{(2-n)}$. Equimolar amounts of H_3BTB-X and -Y (0.050 mmol; 22 mg for **A**, 24 mg for **B**, 29 mg for **C**, 26 mg for **D**, 38 mg for **E**, 27 mg for **F1**, 29 mg for **G**, 25 mg for **H**, 24 mg for **I**, 24 mg for **J**) and $Zn(NO_3)_2{\cdot}6H_2O$ (250 mg, 0.840 mmol) in 10 mL DEF were placed in a 20 mL vial, which was heated at 100 °C for 24 h. Obtained crystals were washed with DEF (3 × 5 mL).

EA data for the as-synthesized samples.

MOF-177-AB: Calcd. for $Zn_4C_{129}H_{196.71}N_{16.71}O_{28}$ = $Zn_4O(BTB)_{1.43}(BTB\text{-}NH_2)_{0.57}{\cdot}(DEF)_{15}$: C, 57.57; H, 7.37; N, 8.70%. Found: C, 56.43; H, 7.58; N, 8.74%.

MOF-177-AC: Calcd. for $Zn_4C_{129}H_{194.07}N_{15.93}O_{29.86}$ = $Zn_4O(BTB)_{1.69}(BTB\text{-}NO_2)_{0.31}{\cdot}(DEF)_{15}$: C, 57.23; H, 7.22, N, 8.24%. Found: C, 55.96; H, 7.53, N, 8.33%.

MOF-177-AD: Calcd. for $Zn_4C_{130.89}H_{198.78}N_{15}O_{29.89}$ = $Zn_4O(BTB)_{1.37}(BTB\text{-}OCH_3)_{0.63}{\cdot}(DEF)_{15}$: C, 57.75; H, 7.36; N, 7.72%. Found: C, 56.52; H, 7.73; N, 8.09%.

MOF-177-AE: Calcd. for $Zn_4C_{128.66}H_{181.28}N_{13}O_{27.38}$ = $Zn_4O(BTB)_{1.54}(BTB\text{-}OC_7H_7)_{0.46}{\cdot}(DEF)_{13}$: C, 59.21; H, 7.00; N, 6.98%. Found: C, 61.52; H, 6.93; N, 5.98%.

MOF-177-AF1: Calcd. for $Zn_4C_{129}H_{191.76}N_{15}O_{28}F_{3.24}$ = $Zn_4O(BTB)_{1.46}(BTB\text{-}(F)_2)_{0.54}{\cdot}(DEF)_{15}$: C, 56.88; H, 7.10; N, 7.71%. Found: C, 55.51; H, 7.58; N, 7.77%.

MOF-177-AG: Calcd. for $Zn_4C_{132.52}H_{188.26}N_{14}O_{27}$ = $Zn_4O(BTB)_{1.29}(BTB\text{-}C_4H_4)_{0.71}{\cdot}(DEF)_{14}$: C, 59.59; H, 7.10; N, 7.34%. Found: C, 58.63; H, 7.64; N, 7.61%.

MOF-177-AH: Calcd. for $Zn_4C_{124}H_{181.51}N_{14}O_{27}F_{2.49}$ = $Zn_4O(BTB)_{1.17}(BTB\text{-}F)_{0.83}{\cdot}(DEF)_{14}$: C, 57.08; H, 7.01; N, 7.52%. Found: C, 55.87; H, 7.62; N, 7.96%.

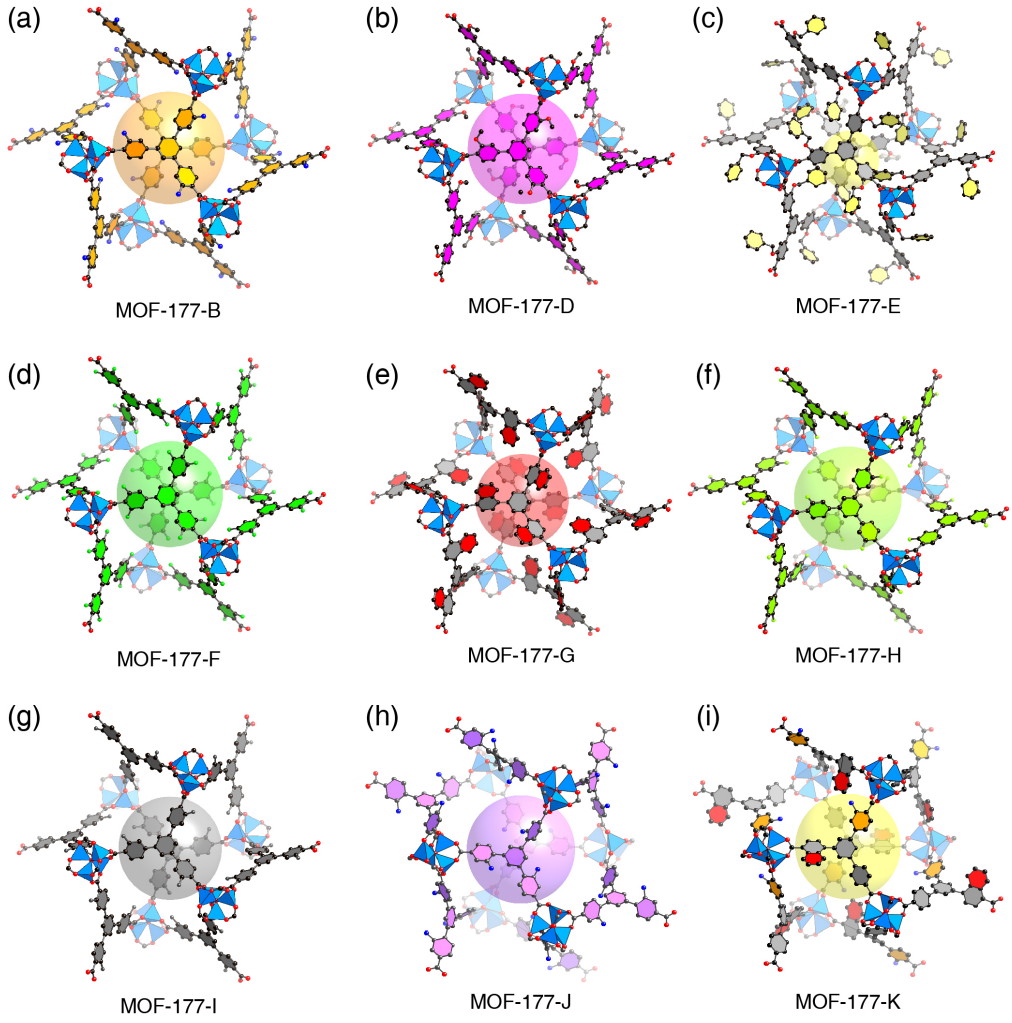

Figure 1. Crystal structures of MOF-177compounds synthesized from linkers with various functional groups. All of these MOFs made of pure linkers have the same **qom** topology as MOF-177. Atom colors: C, black; O, red; N, blue; F, light green; Zn, blue polyhedra; H atoms were omitted for clarity. Large color sphere represent voids in the structures.

MOF-177-AI: Calcd. for $Zn_4C_{126.49}H_{188.98}N_{15}O_{27}$ = $Zn_4O(BTB)_{1.17}(BTB\text{-}Me)_{0.83}\cdot(DEF)_{14}$: C, 58.45; H, 7.33; N, 7.54%. Found: C, 57.44; H, 7.96; N, 7.95%.

MOF-177-AJ: Calcd. for $Zn_4C_{124}H_{185.8}N_{15.8}O_{27}$ = $Zn_4O(BTB)_{1.40}(BTB\text{-}m NH_2)_{0.60}\cdot(DEF)_{14}$: C, 57.47; H, 7.23; N, 8.54%. Found: C, 55.63; H, 7.63; N, 8.98%.

MOF-177-BC: Calcd. for $Zn_4C_{129}H_{196.08}N_{21}O_{32.92}$ = $Zn_4O(BTB\text{-}NH_2)_{1.18}(BTB\text{-}NO_2)_{0.82}\cdot(DEF)_{15}$: C, 54.76; H, 6.99; N, 10.40%. Found: C, 52.94; H, 7.80; N, 10.12%.

MOF-177-BG: Calcd. for $Zn_4C_{140.52}H_{203.88}N_{18.2}O_{28}$ = $Zn_4O(BTB\text{-}NH_2)_{1.04}(BTB\text{-}C_4H_4)_{0.96}\cdot(DEF)_{15}$: C, 59.08; H, 7.19; N, 8.88%. Found: C, 57.02; H, 8.20; N, 8.75%.

MOF-177-CG: Calcd. for $Zn_4C_{145.56}H_{201.42}N_{16.86}O_{31.72}$ = $Zn_4O(BTB\text{-}NO_2)_{0.62}(BTB\text{-}C_4H_4)_{1.38}\cdot(DEF)_{15}$: C, 59.13; H, 6.87; N, 7.99%. Found: C, 58.80; H, 7.48; N, 7.85%.

To yield guest-free materials, MOF-177-XY (-AB, -AC, -AD, -AE, -AF1, and -AG) were fully exchanged with anhydrous acetone (3 × 10 mL for 3 days) and further activated by the SCD method.

MTV-MOF-177-AF2, $Zn_4O(BTB)_{1.21}(BTB\text{-}(F)_2)_{0.79}$. A mixture of the acid form of **A** (13 mg, 0.030 mmol), the acid form of **F** (38 mg, 0.070 mmol) and $Zn(NO_3)_2\cdot 6H_2O$ (250 mg, 0.840 mmol) was dissolved in 10 mL DEF in a 20 mL vial, which was heated at 100 °C for 24 h. Colorless block-shaped crystals were isolated and washed with DEF (3 × 5 mL). EA for the as-synthesized sample of MOF-177-AF2: Calcd. for $Zn_4C_{124}H_{179.26}N_{15}O_{27}F_{4.74}$ = $Zn_4O(BTB)_{1.21}(BTB\text{-}(F)_2)_{0.79}\cdot(DEF)_{14}$: Calcd. C, 56.21; H, 6.82; N, 7.40%. Found: C, 55.09; H, 7.44; N, 7.70%. To yield guest-free material, MOF-177-AF2 was fully exchanged with anhydrous acetone (3 × 10 mL for 3 days) and further activated by the SCD method.

MTV-MOF-177-ABG, $Zn_4O(BTB)_{1.03}(BTB\text{-}NH_2)_{0.31}(BTB\text{-}C_4H_4)_{0.66}$. A mixture of the acid form of **A** (15 mg, 0.33 mmol), the acid form of **B** (16 mg, 0.33 mmol), the acid form of **G** (19 mg, 0.33 mmol), and $Zn(NO_3)_2\cdot 6H_2O$ (250 mg, 0.840 mmol) was dissolved in 10 mL DEF in a 20 mL vial, which was heated at 100 °C for 24 h. Obtained crystals were washed with DEF (3 × 5 mL). To yield guest-free material, MOF-177-ABG was fully exchanged with anhydrous acetone (3 × 10 mL for 3 days) and further activated by the SCD method. EA for activated sample of MOF-177-ABG: Calcd. for $Zn_4C_{61.92}H_{34.89}N_{0.93}O_{13}$ = $Zn_4O(BTB)_{1.03}(BTB\text{-}NH_2)_{0.31}(BTB\text{-}C_4H_4)_{0.66}$: Calcd. C, 58.96; H, 2.79; N, 1.03%. Found: C, 58.15; H, 2.19; N, 0.90%.

RESULTS AND DISCUSSION

Design Strategy for the Functionalization of BTB Linkers. In order to investigate the influence of linker functionalization on MOF-177, we prepared ten different functionalized BTB linkers that were chemically distinct and which had varying strength of inductive effects and steric congestion (Scheme 2). All functionalities incorporated were attached to the peripheral benzoate units as opposed to the central benzene of the BTB linker. Eight of these BTB derivatives were functionalized at the *ortho*-position (R_1 or with additional R_2, Scheme 2) with electron-donating groups (-NH_2, -OCH_3, -OC_7H_7, and -CH_3) or electron-withdrawing groups [-NO_2, -$(F)_2$, -C_4H_4, and -F]. The sizes of the functional groups also varied. Bulky substituents, such as -OC_7H_7 and -C_4H_4, were chosen to study steric effects. Furthermore, the same functional group (e.g. -NH_2) was applied at different positions of the linker (*ortho*-, R_1, and *meta*-, R_3, for linker **B** and **J**, respectively) in order to study how the conformation of the linker was imparted by functional groups at these positions. This has been noted as critical for the design of MOFs with different topologies.[13] Finally, we further explored the possibility of building the MOF-177 structure, with the **qom** net, using a variety of functional groups on one linker (e.g. linker **K** with -H, -NH_2 and -C_4H_4 on each of the three peripheral benzoate units).

Functionalization of the MOF-177 Structure. A series of nine MOF-177-X structures, composed of only one type of linker, were synthesized using the ten functionalized BTB linkers, **B**-**K** except for **C** (Figure 1). Through SXRD analysis, all nine MOF-177-X structures were found to have crystalized in the same trigonal space group ($P\bar{3}1c$), have similar unit cell parameters with respect to one another, and were confirmed to be isoreticular to MOF-177-A (SI, Section S2). For each of these single-crystal structures, two $Zn_4O(\text{-}COO)_6$ clusters and three tritopic BTB linkers, with the respective functionalities, were crystallographically independent and their location and connectivity were well resolved to elucidate the **qom** net. These findings demonstrated that the MOF-177 structure is, in fact, tolerant to a wide range of functionalities with respect to steric congestion and inductive effects imposed on the BTB linker.

A detailed analysis of the linker conformation in each single-crystal structure of this MOF-177 series was performed (SI, section 2). Specifically, two dihedral angles were calculated and tabulated (Table S14): the angle between the peripheral benzoate units and the central benzene (ϕ, Figure S15) and the angle between the peripheral benzene and carboxylate (ψ, Figure S15). It was found that the rotation of the ϕ angle was critical to adjust for the different functionalities incorporated. Due to a slight rotational disorder resulting from multiple independent linkers in the structure, the ϕ angle is represented as an average. Relatively large ϕ angles were observed in MOF-177-G and -J (65.8° and 52.7°, respectively), which significantly differed from that of the pristine MOF-177-A (36.9°). This is attributed to steric hindrance resulting from functionalization at the R_3 position. Although linker **E** incorporates a bulky -OC_7H_7 group at the R_1 position, the dihedral angle in MOF-177-E was quite small (32.0°). These two results indicate that functional groups at the *meta*-position (R_3) of the peripheral benzoate units imposed greater steric restriction to the free rotation of the benzoate; therefore the conformation of the respective linkers has to be significantly altered in order to adopt the **qom** net. This is in contrast to the functional groups at the *ortho*-position. A quantitative molecular mechanics calculation on a discrete BTB linker molecule suggested that even a small *meta*-NH_2 group could impose a large energy barrier to the free rotation of the peripheral benzoate unit (> 100 kcal/mol, Figure S16). The energy-minimal dihedral angle between the peripheral benzoate and the central benzene in the free molecule of linker **J** was found to be 65.2°, which is distinctly different from that of the pristine linker **A** (41.7°).

In addition to steric congestion, we also note the influence that inductive effects play when certain functionalized linkers are introduced into the synthesis. In general, electron-withdrawing groups will facilitate deprotonation (increase acidity), but meanwhile will weaken the coordination ability of the carboxylate moiety of the linker.[14] For example, MOF-177-F, which incorporated the electron-withdrawing group -$(F)_2$, could only be realized using only low concentrations of linker **F**. At higher concentrations, MOF-155-F with **pyr** net was the predominate product. In the case of the stronger electron-withdrawing group, -NO_2, the reactivity of linker **C** was observed to be significantly lower than that of linker **F**, which unfortunately prevented the realization of MOF-177-C even after exhaustive efforts were undertaken. This observation is reminiscent of the MOF-5 structure, in which the -NO_2 functionalized ditopic linker (the same functionality as in linker **C**) was unable to be introduced without the presence of a second ditopic linker.[10a] It is plausible that the *ortho*-positioned -NO_2 group is also capable of orientating to other clusters, as was found in the $Zn_7O_2(\text{-}COO)_{10}$ cluster in MOF-123, rather than $Zn_4O(\text{-}COO)_6$, thus preventing the formation of the MOF-177 structure.[15]

Linker F and J select for pyr and rtl rather than qom net. Although the MOF-177 architecture was realized for all, but one, linkers employed in this study, topological diversity was still observed in the MOF synthesis, specifically when linkers **F** and **J** were employed alone.

MOF-155-F. Cubic-shaped crystals of MOF-155 were obtained under the same synthetic conditions used for MOF-177-A, but different in that linker **F** is substituted for linker **A**. The single crystal X-ray structure of MOF-155 shows that this isomeric structure crystallizes in the cubic $Ia\bar{3}$ space group with an axis length of 25.9639(7) Å. In this structure, octahedral $Zn_4O(\text{-}COO)_6$ units are linked by tritopic BTB-$(F)_2$ linkers to afford a three-dimensional framework having a **pyr** net (Figure 2a). Furthermore, MOF-155 consists of two-fold interpenetrating frameworks, which leads to a bicontinuous channel with a smaller internal pore diameter of 8 Å.

MOF-156-J. Needle-shaped crystals were obtained under the same synthetic conditions used for MOF-177-A, but using linker **J** instead of linker **A**. This MOF has a tetragonal $P4_2/mnm$ space group with axis lengths of a = 24.360(3) and c = 16.909(3) Å. The underlying net of this MOF is **rtl**, which is that of rutile: the Ti and O atoms are replaced by $Zn_4O(\text{-}COO)_6$ units and linker **J**, respectively, to produce square channels of 9 Å in diameter (Figure 2b).

MOF-155-J. Interestingly, another MOF based on **pyr** was also observed when using linker **J** alone (Scheme 2). This phase is a byproduct during the synthesis of MOF-177-J and MOF-155-J. MOF-155-J crystallizes in the cubic $Pa\bar{3}$ space group with an axis length of 25.888(3) Å (Figure S12 and Table S12). This structure also has the same **pyr** net topology, but consists of two interpenetrating frameworks.

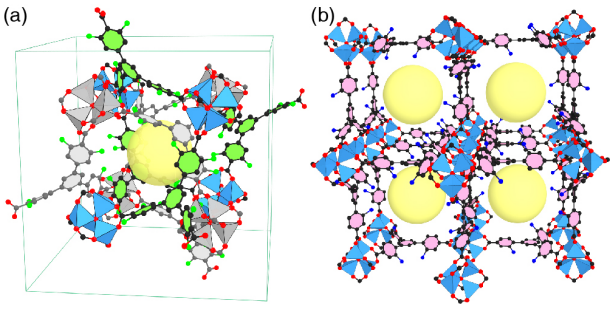

Figure 2. Crystal structure of MOF-155-F made from linker **F** in doubly interpenetrated **pyr** net (a) and crystal structure of MOF-156-J made from linker **J** forming the **rtl** net (b). Atom colors: C, black; O, red; N, blue; F, green; Zn, blue polyhedra; H atoms were omitted for clarity. The interpenetrating framework (green hexagons linked by blue polyhedral) in (a) is also depicted. Atom colors: Zn, grey polyhedra and C, grey. The large yellow sphere represents the void in the structure.

Aside from the expected inductive effects, the relative positions of the functionalities on the BTB linker can impact the conformation of the linker structure, as evidenced by the varying linker conformations observed in these topologically diverse MOFs. When comparing the linker conformations in the different topologies, it is suggested that in the **pyr** net (MOF-155-F and -J), the linkers **F** and **J** experience a slight distortion and deviate from the molecular plane that is defined by the three carbon atoms from the three carboxylate groups (Figure S18). Upon careful analysis of linker **J** in the **rtl** net (MOF-156-J), distortion of the linker was not observed (Figure S19), however, differences in linker orientation accompanied by distortion of the SBU were (Figures S20 and S21). Since the **qom** net can also be derived from these linkers, the design of the linker was not solely consequential for determining the resulting topologies in these cases. Nevertheless, synthetic conditions (dilution of reactant concentration or using different solvent systems altogether) and the MTV approach were the most viable means for obtaining control over the observed topological diversity.

Multivariate (MTV) Metal-Organic Framework-177: Incorporation of Multiple Functionalities within the Same Framework. Fourteen MTV-MOF-177 compounds were prepared by mixing two or three types of linkers. This strategy was used in order to assess how the introduction of multiple functional groups in varying ratios within the pores of MOF-177-A impacts gas properties when compared to that of the parent MOF-177-A structure (Scheme 1). For the binary MTV-MOF-177 compounds, ten were composed of BTB and one functionalized BTB linker (MTV-MOF-177-AB, -AC, -AD, -AE, -AF1, -AF2, -AG, -AH, -AI, and -AJ) and three were composed of two different functionalized BTB linkers (MTV-MOF-177-BC, -BG, and -CG). Furthermore, a ternary system of MTV-MOF-177-ABG was prepared by combining two functionalized BTB linkers (**B** and **G**) with the pristine BTB linker (**A**) to illustrate the application of the MTV approach to the structure of MOF-177. The successful formation of highly crystalline and phase-pure MTV-MOF-177 structures was confirmed by PXRD analyses of the as-synthesized samples (SI, Section S3). Once the phase purity was confirmed, the ratios of the linkers in the MTV-MOF-177 derivatives were estimated from ^{1}H NMR spectra of their acid-digested samples (SI, Section S5). We describe the characterization of MTV-MOF-177-ABG as a representative for all of the MTV-MOF-177 materials.

The PXRD pattern of MTV-MOF-177-ABG is shown in Figure 3. To limit the contribution of solvent in the X-ray diffraction pattern, MTV-MOF-177-ABG was activated. This process allowed for the collection of a higher quality PXRD pattern. No extra diffraction peaks were observed from the experimental PXRD pattern in comparison with the simulated pattern generated from the structural model of MOF-177-A. It is noted that only a small difference in intensities were realized after the convergence of Pawley refinement (R_{wp} = 17%; R_p = 12%), which took into account the space group (Trigonal $P\bar{3}1c$) and unit cell parameters (a = 38.123, c = 30.632 Å).

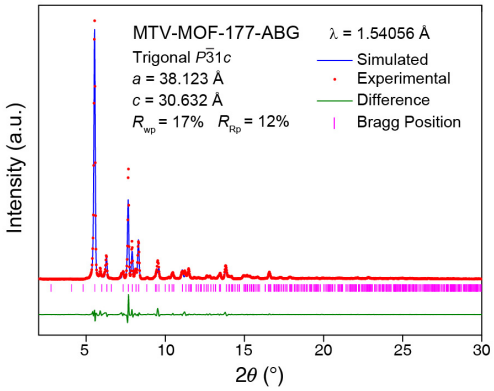

Figure 3. PXRD pattern of activated (red) MTV-MOF-177-ABG sample and the profile fitting using Pawley refinement (blue).The difference plot (green) and Bragg position (magenta) are also displayed as references overlaid.

Next, an activated sample (*ca.* 10 mg) of MTV-MOF-177-ABG was dissolved in DMSO-d_6 (deuterated dimethyl sulfoxide, 580 μL) and 20% DCl in D_2O (20 μL) for ^{1}H NMR analysis. The proton signals from each linker can be assigned based on the chemical shifts and their inherent splitting patterns (Figure 4). The linker ratio for **A**:**B**:**G** was calculated to be 1.00:0.32:0.62, which is different from the input ratio used in the reaction mixture (elaborated below). The formula of MTV-MOF-177-ABG was thus estimated as $Zn_4O(BTB)_{1.03}(BTB\text{-}NH_2)_{0.31}(BTB\text{-}Nap)_{0.66}$ and further confirmed by EA (see Experimental Section).

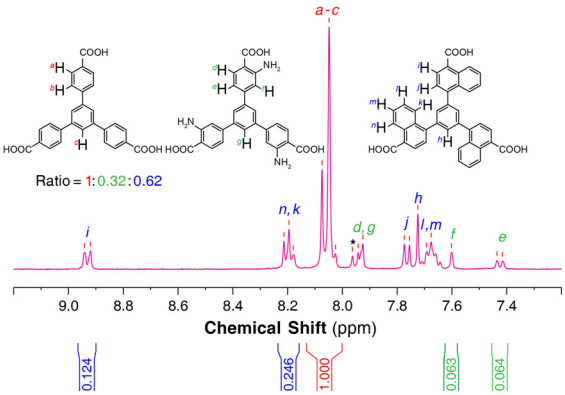

Figure 4. ^{1}H NMR spectrum of MTV-MOF-177-ABG demonstrating the linker ratio in the MOF backbone. All three linkers are present with significant occupancy. The chemical shifts were assigned to each corresponding linkers and the integration were used for the calculation of linker ratio.

Control of Linker Ratios in Binary MTV-MOF-177. The relative ratios of the various linkers incorporated within the framework were quantitatively examined in digested MOFs by NMR spectroscopy. The relationships between the input ratio, based on the concentration of linkers used in the synthesis, and the output ratio, based on the concentration of linkers observed in the MOF crystals, were systematically studied in four selected MTV-MOF-177 structures composed of two unique linkers (-AB, -AC, -AF, and –AG; Figure 5). From this, a clear trend is observed of the output linker ratio in the resulting MTV-MOF crystal increasing when a higher input ratio of the corresponding linker was applied in the starting solution of the reaction.

There is a clear deviation from the linear relationship that is expected in an ideal scenario of output ratio being equal to that of the input. However, a general trend is noted of linker **A** being incorporated more readily than other functionalized linkers. In every examined MTV-MOF containing linker **A**, the amount of **A** was always higher than the other linkers in the frameworks. The preferred incorporation of linker **A** is most likely a result of the linker's flexibility of rotation to adopt the MOF-177 structure (Figures S16 and S17), however, many other factors, including reaction kinetics and substituent effects, may also play important roles for this.

It is worth noting that by employing the multivariate strategy, linker **C** can be incorporated into the MOF-177 structure and in significant amounts (higher than 60% when accompanied by linker **A**, Figure 5) by manipulating the input linker ratios during the synthesis. This is interesting given the fact that it proved difficult, if not impossible, to construct an isoreticular MOF-177 structure when linker **C** was used alone. Although an output ratio cannot be predicted *a priori*, a reproducible input/output relationship diagram can be constructed (Figure 5). This proves beneficial when a targeted functional group is needed with a desired concentration in the MOF crystal.

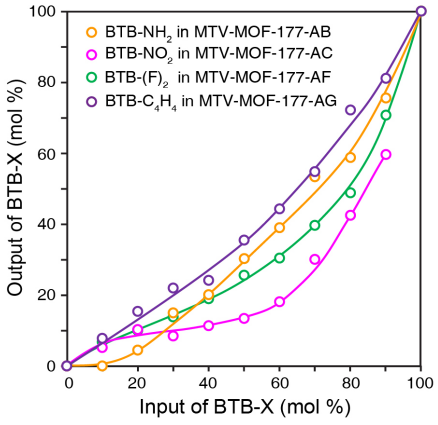

Figure 5. Diagram demonstrating the relationship between input ratios and output ratios of various functionalized linkers in MTV-MOF-177-AB (orange), -AC (magenta), -AF (green), and -AG (purple), respectively. As the input ratio increases, the presence of linker in the MTV-MOF backbone also increases, albeit in a nonlinear relationship.

Permanent Porosity and Hydrogen Adsorption Capacity. Before the gas adsorption measurements were conducted, the void fraction and geometrical surface area of the single-linker-based MOF-177-X series were estimated (Table 1). As is shown, there is a rough trend based on the relationship between porosity and the size of functional groups included within the framework; MOF-177-X structures having smaller functional groups (e.g. MOF-177-B, -D and -J) exhibit greater geometric surface areas when compared to MOF-177-X structures with bulky functionalities (e.g. MOF-177-G and -E). Remarkably, due to the high porosity of original MOF-177-A, it is clear that these isostructural frameworks are capable of retaining high porosity even upon addition of functionalities within the pores.

The porosity of the MOF-177-X isostructural series was experimentally proven by N_2 adsorption measurements at 77 K (Figure 6a). All examined MOF-177-X materials displayed significant N_2 uptake in the low-pressure region ($P/P_0 < 0.05$) and near saturation was observed at $P/P_0 = 0.2$, which is indicative of permanent microporosity. The profiles of the isotherms are all classified as Type I. Additionally, all of these materials exhibit high BET surface areas (large pore volumes) [3800 m^2/g (1.63 g/cm^3), 2650 m^2/g (1.53 g/cm^3), 3690 m^2/g (1.53 g/cm^3), 3480 m^2/g (1.68 g/cm^3) for MOF-177-B, -D, -F, and -I, respectively]. These values are close to those that were geometrically calculated from their structural models (Table 1). As a reference, the Langmuir surface areas of MOF-177-X analogs are also listed in Table 1. However, these values are lower than those of unfunctionalized MOF-177-A due to their smaller void fraction and larger crystal density.

The high N_2 (Ar) uptake capacity at 77 K (87 K) is also observed for the MTV-MOF-177 compounds (Figure 6b); these MOF materials showed Type I isotherms with no significant accompanied hysteresis. The BET surface areas were calculated to be 3950, 2430, 2740, 3330, 4315, 4170, 4000, and 3490 m^2/g for MTV-MOF-177-AB, -AC, -AD, -AE, -AF1, -AF2, -AG, and -ABG, respectively. A noticeable trend is observed in that the estimated surface areas are proportional to the pore volume and the surface areas are less sensitive to the functionalities in the MOF structures (Table 1).

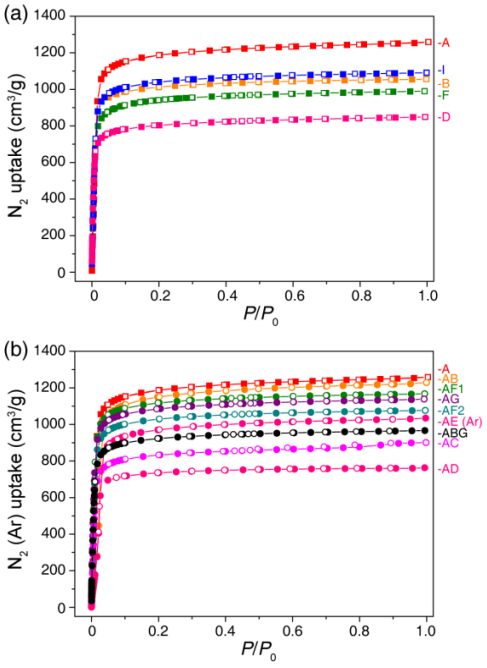

Figure 6. N_2 (Ar) adsorption isotherms at 77 K (87 K) for MOF-177 analogs (a) and MTV-MOF-177 derivatives (b) showing that all MOFs have permanent porosity and high surface area after activation.

Low-pressure hydrogen isotherms of MTV-MOF-177 derivatives were recorded at 77 K (Figure 7). The hydrogen uptake gradually increased with an increase in the pressure, while no saturation uptake was observed under the present experimental conditions. An increase in volumetric hydrogen uptake was generally observed in all the MTV-MOF-177 derivatives in comparison with the unfunctionalized MOF-177-A parent structure. It is worth noting that the MOF-177-B and MOF-177-D are observed to have 25% higher H_2 volumetric uptake than that of the MOF-177-A at 800 Torr.

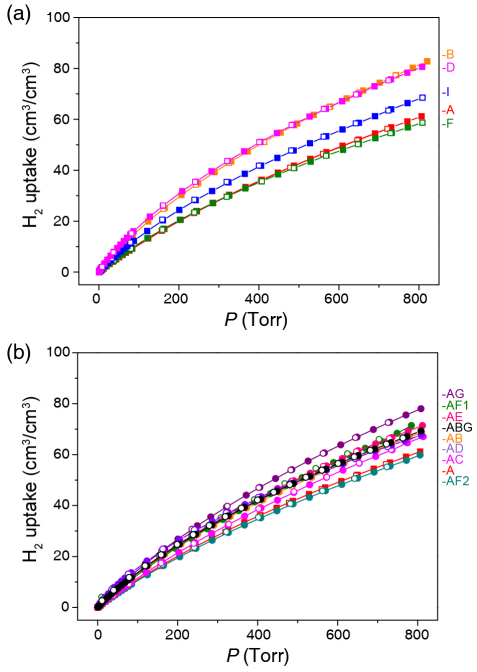

Figure 7. Volumetric H_2 uptake at 77 K for MOF-177-X (a) and MTV-MOF-177 compounds (b). A maximum 25% increase of H_2 uptake can be observed with MOF-177-B and -D, when $-NH_2$ and $-OCH_3$ functional groups are introduced respectively.

A high-pressure methane adsorption isotherm for MTV-MOF-177-AF1 was recorded at 298 K (Figure 8). The methane uptake behavior of MTV-MOF-177-AF1 is similar to that of the unfunctionalized MOF-177-A, which exhibits roughly 210 cm^3/cm^3 (150 g/L) at 80 bar and 298 K.

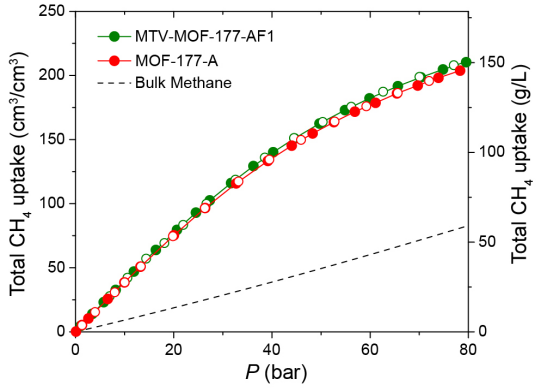

Figure 8. Volumetric CH_4 total uptake at 298 K for MTV-MOF-177-AF1 (green) compared with those of the MOF-177-A (red) and the bulk methane (black).

SUMMARY

In this work, we have functionalized the highly porous MOF-177 structure through the incorporation of one or multiple types of functionalized tritopic linkers. We have demonstrated that MOF-177 with the **qom** topology is quite tolerant to a wide range of functional groups. However, topological diversity and phase selection was observed as a function of the positioning of the functional group on the BTB linker. The MTV approach allowed the systematic investigation of multivariate materials with varying ratios of multiple functionalities. In turn, this provided motivation for uncovering the trend of disproportional incorporation of different linkers in the synthesis, which enables the customized production of MTV-MOF-177 structures with specific ratios of desirable functionalities. Adsorption studies on selected MOF-177 analogs and derivatives showed the retention of its high surface area and revealed an enhancement in hydrogen uptake.

On a fundamental level, we have shown that (a) the position of functionality on an organic linker codes for certain MOFs of a specific topology, (b) a specific functionality, which could not be introduced into a specific structure can be successfully introduced into the desired MOF structure by the MTV approach, and (c) the presence of more than one kind of functionality in MOFs leads to enhancement of gas adsorptive properties where the whole performs better than the sum of the parts.

ASSOCIATED CONTENT

Supporting Information. Linker syntheses and characterization, SXRD data, linker conformations, molecular mechanics energy calculations, PXRD patterns, TGA curves, NMR spectroscopy, adsorption isotherms, and CIF files. This material is available free of charge via the Internet at http://pubs.acs.org.

AUTHOR INFORMATION

Corresponding Authors

hdeng@whu.edu.cn; jaheon@ssu.ac.kr; yaghi@berkeley.edu

Notes

The authors declare no competing financial interest.

ACKNOWLEDGMENT

This work was partially supported for synthesis by U.S. Department of Energy, Office of Science, Office of Basic Energy Sciences, Energy Frontier Research Center (DE-SC0001015), characterization by KACST (Saudi Arabia), and gas adsorption by BASF SE (Ludwigshafen, Germany). We acknowledge Drs. S. K. Dey, C. Valente, and Prof. J. F. Stoddart (Northwestern University) for preliminary work on the synthesis of the links; Drs. S. Teat and K. Gagnon for the synchrotron X-ray diffraction data acquisition support at the beamline 11.3.1 (Advanced Light Source, Lawrence Berkeley National Laboratory); Drs. F. Gándara (Yaghi group) and C. B. Knobler (UCLA) for support in X-ray crystallography; and Drs. A. C.-H. Sue, M. Suzuki, A. M. Fracaroli, J. Yuan (Yaghi group), and Mr. J. Park (KAIST, Republic of Korea) for support in the sample preparation and characterization. J.K. thanks the support by the Korea CCS R&D Center grant funded by the Ministry of Science, ICT & Future Planning (NRF-2012-0008900), and the Pohang Accelerator Laboratory for the X-ray data collection (Republic of Korea).

Table 1. Porosity data for MOF-177-X and MTV-MOF-177 compounds.

Compound	Formula	Crystal density (g/cm^3)	A_{BET} (m^2/g)	A_{Lang} (m^2/g)	A_{geo}[a] (m^2/g)	V_p (cm^3/g)
MOF-177-A	$Zn_4O(BTB)_2$	0.43	4740	5340	4800	1.89
MOF-177-B	$Zn_4O(BTB\text{-}NH_2)_2$	0.46	3800	4620	4530	1.63
MOF-177-D	$Zn_4O(BTB\text{-}OCH_3)_2$	0.49	2650	3560	4510	1.53
MOF-177-E	$Zn_4O(BTB\text{-}OC_7H_7)_2$	0.66	ND	ND	2880	ND
MOF-177-F	$Zn_4O(BTB\text{-}(F)_2)_2$	0.51	3690	4345	3980	1.53
MOF-177-G	$Zn_4O(BTB\text{-}C_4H_4)_2$	0.54	ND	ND	4350	ND
MOF-177-H	$Zn_4O(BTB\text{-}F)_2$	0.47	ND	ND	4360	ND
MOF-177-I	$Zn_4O(BTB\text{-}CH_3)_2$	0.46	3480	4760	4360	1.68
MOF-177-J	$Zn_4O(BTB\text{-}m NH_2)_2$	0.46	ND	ND	4810	ND
MOF-177-K	$Zn_4O(BTB\text{-}C_4H_4/NH_2)_2$	0.48	ND	ND	4570	ND
MTV-MOF-177-AB	$Zn_4O(BTB)_{1.43}(BTB\text{-}NH_2)_{0.57}$	0.44	3950	4700	ND	1.54
MTV-MOF-177-AC	$Zn_4O(BTB)_{1.69}(BTB\text{-}NO_2)_{0.31}$	0.45	2430	3727	ND	1.39
MTV-MOF-177-AD	$Zn_4O(BTB)_{1.37}(BTB\text{-}OCH_3)_{0.63}$	0.45	2740	3340	ND	1.18
MTV-MOF-177-AE	$Zn_4O(BTB)_{1.54}(BTB\text{-}OC_7H_7)_{0.46}$	0.48	3330	3960	ND	1.29
MTV-MOF-177-AF1	$Zn_4O(BTB)_{1.46}(BTB\text{-}(F)_2)_{0.54}$	0.45	4315	5110	ND	1.79
MTV-MOF-177-AF2	$Zn_4O(BTB)_{1.21}(BTB\text{-}(F)_2)_{0.79}$	0.46	4170	4710	ND	1.66
MTV-MOF-177-AG	$Zn_4O(BTB)_{1.29}(BTB\text{-}C_4H_4)_{0.71}$	0.47	4000	4870	ND	1.76
MTV-MOF-177-AH	$Zn_4O(BTB)_{1.17}(BTB\text{-}F)_{0.83}$	0.45	ND	ND	ND	ND
MTV-MOF-177-AI	$Zn_4O(BTB)_{1.17}(BTB\text{-}CH_3)_{0.83}$	0.44	ND	ND	ND	ND
MTV-MOF-177-AJ	$Zn_4O(BTB)_{1.40}(BTB\text{-}m NH_2)_{0.60}$	0.44	ND	ND	ND	ND
MTV-MOF-177-BC	$Zn_4O(BTB\text{-}NH_2)_{1.18}(BTB\text{-}NO_2)_{0.82}$	0.49	ND	ND	ND	ND
MTV-MOF-177-BG	$Zn_4O(BTB\text{-}NH_2)_{1.04}(BTB\text{-}C_4H_4)_{0.96}$	0.50	ND	ND	ND	ND
MTV-MOF-177-CG	$Zn_4O(BTB\text{-}NO_2)_{0.62}(BTB\text{-}C_4H_4)_{1.38}$	0.54	ND	ND	ND	ND
MTV-MOF-177-ABG	$Zn_4O(BTB)_{1.03}(BTB\text{-}NH_2)_{0.31}(BTB\text{-}C_4H_4)_{0.66}$	0.47	3490	4122	ND	1.49

[a] A_{BET}, A_{Lang}, and A_{geo} are the BET, Langmuir, and geometric surface areas, respectively. V_p is the measured pore volume. ND, no data. Geometric surface areas were calculated using *Materials Studios 5.0* with the N_2 as probe (diameter 3.681 Å) according to published procedure.[16]

REFERENCES

(1) (a) Furukawa, H.; Cordova, K. E.; O'Keeffe, M.; Yaghi, O. M. *Science* **2013**, *341*, 974. (b) Ferey, G. *Chem. Soc. Rev.* **2008**, *37*, 191. (c) Lu, W.; Wei, Z.; Gu, Z.-Y.; Liu, T.-F.; Park, J.; Park, J.; Tian, J.; Zhang, M.; Zhang, Q.; Gentle III, T.; Bosch, M.; Zhou, H.-C. *Chem. Soc. Rev.* **2014**, *43*, 5561. (d) Ramaswamy, P.; Wong, N. E.; Shimizu, G. K. H. *Chem. Soc. Rev.* **2014**, *43*, 5913. (e) Wang, C.; Liu, D.; Lin, W. *J. Am. Chem. Soc.* **2013**, *135*, 13222. (f) Gao, W.-Y.; Chrzanowski, M.; Ma, S.; *Chem. Soc. Rev.* **2014**, *43*, 5841. (g) Senkovskaa, I.; Kaskel, S. *Chem. Commun.* **2014**, *50*, 7089. (h) Lin, X.; Telepeni, I.; Blake, A. J.; Dailly, A.; Brown, C. M.; Simmons, J. M.; Zoppi, M.; Walker, G. S.; Thomas, K. M.; Mays, T. J.; Hubberstey, P.; Champness, N. R.; Schröder, M. *J. Am. Chem. Soc.* **2009**, *131*, 2159. (i) Farha, O. K.; Eryazici, I.; Jeong, N. C.; Hauser, B. G.;Wilmer, C. E.; Sarjeant, A. A.; Snurr, R. Q.; Nguyen, S. T., Yazaydın, A. Ö.; Hupp, J. T. *J. Am. Chem. Soc.* **2012**, *134*, 15016. (j) An, J.; Farha, O. K.; Hupp, J. T.; Pohl, E.; Yeh, J. I.; Rosi, N. L. *Nat. Commun.* **2012**, *3*, 604. (k) Zhang, Y. B.; Zhou, H. L.; Lin, R. B.; Zhang, C.; Lin, J. B.; Zhang, J. P.; Chen, X. M. *Nat. Commun.* **2012**, *3*, 642. (l) Koh, K.; Wong-Foy, A. G.; Matzger, A. J. *Angew. Chem. Int. Ed.* **2008**, *47*, 677. (m) Liu, L.; Konstas, K.; Hill, M. R.; Telfer, S. G. *J. Am. Chem. Soc.* **2013**, *135*, 17731. (n) Brozek, C. K.; Dincă, M. *J. Am. Chem. Soc.* **2013**, *135*, 12886. (o) Kim, M.; Cahill, J. F.; Fei, H.; Prather, K. A.; Cohen, S. M. *J. Am. Chem. Soc.* **2012**, *134*, 18082. (p) Tu, B.; Pang, Q.; Wu, D.; Song, Y.; Weng, L.; Li, Q. *J. Am. Chem. Soc.* **2014**, *136*, 14465. (q) Han, Y.; Qi, P.; Li, S.; Feng, X.; Zhou, J.;Li, H.; Su, S.; Li, X.; Wang, B. *Chem. Commun.* **2014**, *50*, 8057. (r)Bu, F.; Lin, Q.; Zhai, Q.; Wang, L.; Wu, T.; Zheng, S.-T.; Bu, X.; Feng, P. *Angew. Chem. Int. Ed.* **2012**, *51*, 8538. (s) Schoedel, A.; Cairns, A. J.; Belmabkhout, Y.; Wojtas, L.; Mohamed, M.; Zhang, Z.; Proserpio, D. M.; Eddaoudi, M.; Zaworotko, M. J. *Angew. Chem. Int. Ed.* **2013**, *52*, 2902.

(2) Ockwig, N. W.; Delgado-Friedrichs, O.; O'Keeffe, M.; Yaghi, O. M. *Acc. Chem. Res.* **2005**, *38*, 176.

(3) (a) Carlucci, L.; Ciani, G; Proserpio, D. M.; Rizzato, S. *Chem.–Eur. J.* **2002**, *8*, 1520. (b) Gándara, F.; Uribe-Romo, F. J.; Britt, D. K.; Furukawa, H.; Lei, L.; Cheng, R.; Duan, X.; O'Keeffe, M.; Yaghi, O. M. *Chem.–Eur. J.* **2012**, *18*, 10595. (c) Elsaidi, S. K.; Mohamed, M. H.; Wojtas, L.; Chanthapally, A.; Pham, T.; Space, B.; Vittal, J. J.; Zaworotko, M. J. *J. Am. Chem. Soc.* **2014**, *136*, 5072.

(4) Yaghi, O. M.; Davis, C. E.; Li, G.; Li, H. *J. Am. Chem. Soc.* **1997**, *119*, 2861.

(5) (a) Reticular Chemistry Structure Resource (RCSR): http://rcsr.anu.edu.au/. (b) O'Keeffe, M.; Peskov, M. A.; Ramsden, S. J.; Yaghi, O. M. *Acc. Chem. Res.* **2008**, *41*, 1782.

(6) Chae, H. K.; Siberio-Perez, D. Y.; Kim, J.; Go, Y.; Eddaoudi, M.; Matzger, A. J.; O'Keeffe, M.; Yaghi, O. M. *Nature* **2004**, *427*, 523.

(7) Furukawa, H.; Ko, N.; Go, Y. B.; Aratani, N.; Choi, S. B.; Choi, E.; Yazaydin, A. Ö.; Snurr, R. Q.; O'Keeffe, M.; Kim, J.; Yaghi, O. M. *Science*, **2010**, *239*, 424.

(8) (a) Furukawa, H.; Miller, M. A.; Yaghi, O. M. *J. Mater. Chem.* **2007**, *17*, 3197. (b) Lim, D.-W.; Yoon, J. W.; Ryu, K. Y.; Suh, M. P. *Angew. Chem. Int. Ed.* **2012**, *51*, 9814. (c) Dau, P. V.; Cohen, S. M. Cohen *CrystEngComm* **2013**, *15*, 9304.

(9) (a) Chae, H. K.; Kim, J.; Friedrichs, O. D.; O'Keeffe, M.; Yaghi, O. M. *Angew. Chem. Int. Ed.* **2003**, *42*, 3907. (b) Caskey, S. R.; Wong-Foy, A. G.; Matzger, A. J. *Inorg. Chem.* **2008**, *47*, 7751. (c) Eubank, J. F.; Wojtas, L.; Hight, M. R.; Bousquet, T.; Kravtsov, V. C.; Eddaoudi, M. *J. Am. Chem. Soc.* **2011**, *133*, 17532.

(10) (a) Deng, H. X.; Doonan, C. J.; Furukawa, H.; Ferreira, R. B.; Towne, J.; Knobler, C. B.; Wang, B.; Yaghi, O. M. *Science* **2010**, *327*, 846. (b) Kong, X.; Deng, H.; Yan, F.; Kim, J.; Swisher, J. A.; Smit, B.; Yaghi, O. M.; Reimer, J. A. *Science* **2013**, *341*, 882. (c) Yeung, H. H. M.; Li, W.; Saines, P. J.; Köster, T. K. J.; Grey, C. P.; Cheetham, A. K. *Angew. Chem. Int. Ed.* **2013**,

52, 5544. (d) Martí-Gastaldo, C.; Antypov, D.; Warren J. E.; Briggs, M. E.; Chater, P. A.; Wiper, P. V.; Miller, G. J.; Khimyak, Y. Z.; Darling, G. R.; Berry, N. G.; Rosseinsky, M. J. *Nature Chem.* **2014**, *6*, 343. (e) Foo, M. L.; Matsuda, R.; Kitagawa, S. *Chem. Mater.* **2013**, *26*, 310. (f) Park, T.-H.; Koh, K.; Wong-Foy, A. G.; Matzger, A. J. *Cryst. Growth Des.* **2011**, *11*, 2059.

(11) Chen, B. L.; Eddaoudi, M.; Hyde, S. T.; O'Keeffe, M.; Yaghi, O. M. *Science* **2001**, *291*, 1021.

(12) (a) Li, K. H.; Olsan, D. H.; Lee, J. Y.; Bi, W. H.; Wu, K.; Yuen, T.; Xu, Q.; Li, J. *Adv. Funct. Mater.* **2008**, *18*, 2205. (b) Nelson, A. P.; Farha, O. K.; Mulfort, K. L.; Hupp, J. T. *J. Am. Chem. Soc.* **2009**, *131*, 458.

(13) Furukawa, H,; Go, Y. B.; Ko, N.; Park, Y. K.; Uribe-Romo, F. J.; Kim, J. ; O'Keeffe, M.; Yaghi, O. M. *Inorg. Chem.* **2011**, *50*, 9147.

(14) (a) Lu, P.; Wu, Y.; Kang, H.; Wei, H.; Liu, H.; Fang, M. *J. Mater. Chem. A* **2014**, *2*, 16250. (b) Vermoortele, F.; Vandichel, M.; Van de Voorde, B.; Ameloot, R.; Waroquier, M.; Van Speybroeck, V.; De Vos, D. E. *Angew. Chem. Int. Ed.* **2012**, *51*, 4887. (c) Hansch, C.; Leo, A.; Taft, R. W. *Chem. Rev.* **1991**, *91*, 165.

(15) Choi, S. B.; Furukawa, H.; Nam, H. J.; Jung, D. Y.; Jhon, Y. H.; Walton, A.; Book, D.; O'Keeffe, M.; Yaghi, O. M.; Kim, J. *Angew. Chem. Int. Ed.* **2012**, *51*, 879.

(16) Duren, T.; Millange, F.; Ferey, G.; Walton, K. S.; Snurr, R. Q. *J. Phys. Chem. C* **2007**, *111*, 15350.

TOC

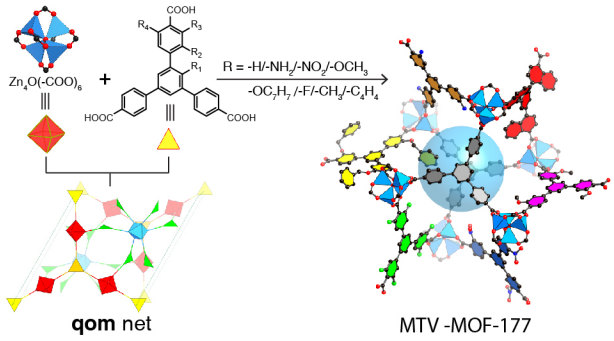
COOH
R4
R3
R2
R1
Zn4O(-COO)6
+
HOOC
COOH
R = -H/-NH2/-NO2/-OCH3
-OC7H7/-F/-CH3/-C4H4
qom net
MTV -MOF-177